

Identification of a New Ultraluminous X-ray Source in NGC 1316

S.Allak,^{1,2}★ A. Akyuz,^{1,3} N. Aksaker,^{1,4} M. Ozdogan Ela,¹ S. Avdan,¹ F. Soyduğan^{2,5}

¹Space Science and Solar Energy Research and Application Center (UZAYMER), University of Ğukurova, 01330, Adana, Turkey

²Department of Physics, University of Ğanakkale Onsekiz Mart, 17100, Ğanakkale, Turkey

³Department of Physics, University of Ğukurova, 01330, Adana, Turkey

⁴Adana Organised Industrial Zones Vocational School of Technical Science, University of Ğukurova, 01410, Adana, Turkey

⁵Astrophysics Research Centre and UlupĞşnar Observatory, University of Ğanakkale Onsekiz Mart, 17100, Ğanakkale, Turkey

Accepted XXX. Received YYY; in original form ZZZ

ABSTRACT

In this study, we report identification of a new ultraluminous X-ray source (ULX) which we named as X-7 in NGC 1316, with an unabsorbed luminosity of 2.10×10^{39} erg s⁻¹ using two recent *Chandra* archival observations. The X-7 was detected in the *Chandra* 2001 observation and it was included in the X-ray source list of the NGC 1316 as CXOUJ032240.8-371224 with luminosity of 5.7×10^{38} erg s⁻¹ implying a luminosity increase of a factor of ~ 4 . The best fit spectral model parameters indicate that X-7 has a relatively hot disk and hard spectra. The mass of compact object is obtained as $\sim 8 M_{\odot}$ which is in the range of a stellar-mass black hole. The X-7 shows a relatively long-term count rate variability while no short-term variability is observed. We also identified a unique optical candidate within 0.''22 error circle at 95% confidence level for X-7 using the archival *HST*/ACS and *HST*/WFC3 data. Absolute magnitude (M_V) of this candidate is -7.8 mag. Its spectral energy distribution is adequately fitted a blackbody model with a temperature of 3100 K indicating an M type supergiant, assuming the donor star dominates the optical emission. In addition, we identified a transient ULX candidate (XT-1) has a high luminosity of $\sim 10^{39}$ erg s⁻¹ located 6'' away from X-7 with no visible counterpart(s).

Key words: galaxies: individual (NGC 1316) X-rays: binaries X-rays: general

1 INTRODUCTION

Ultraluminous X-ray sources (ULXs) are described as off-nuclear point-like objects with high X-ray luminosities in the range of $10^{39} - 10^{41}$ erg s⁻¹ in external galaxies (see the review by Kaaret et al. 2017). For most, their high luminosities are thought to be produced by super-Eddington accretions onto stellar mass black holes or neutron stars (Poutanen et al. 2013; Sutton et al. 2013; Bachetti et al. 2013; Israel et al. 2017a). For some, sub-Eddington accretions onto intermediate mass black holes (IMBH) are possible (Colbert & Mushotzky 1999; Madau & Rees 2001; Mezcua et al. 2015). Actually, numerous studies have examined the nature of the ULX systems, ULX X-2 of M82 with its coherent pulsations was the first neutron star in such systems (Bachetti et al. 2014). Since then, the number of known pulsating ultraluminous X-ray sources (PULXs) has risen to 7. One of them was discovered through a cyclotron resonance scattering feature in the X-ray spectrum of the source by Brightman et al. (2018) and remaining others, through the X-ray detection of their pulsations (Fürst et al. 2016; Israel et al. 2017a,b;

Carpano et al. 2018; Sathyaprakash et al. 2019; Rodríguez Castillo et al. 2019).

High quality data from *XMM-Newton* and *Chandra* revealed that the spectra of ULXs are different from those observed in the Galactic black hole binaries (GBHBs). The most notably feature in the spectra of ULXs is an unambiguous curvature between 3 to 7 keV. This curvature can be produced through Comptonization of a cold, optically thick corona around the compact object or alternatively in the inner regions of a geometrically thick accretion disk (Stobbart et al. 2006; Roberts 2007; Gladstone et al. 2009). Based on these spectral features, a new ultraluminous accretion state with super-Eddington accretion occurring onto a black hole or a neutron star has been proposed by Gladstone et al. (2009). The extended high energy interval of *NuSTAR* observations of ULXs clarified that the curvature was extending above 10 keV. This feature is also different from GBHB, whose cutoff energy is over 60 keV (Bachetti et al. 2013; Luangtip et al. 2016; Pintore et al. 2017; Fürst et al. 2017).

Determining the optical counterpart of ULXs plays an important role to understand the origin of emission (i.e., accretion disk and/or donor star) and to estimate the mass, age and spectral type of the donor. Identification of the optical counterpart of ULXs is

★ E-mail:0417allaksinan@gmail.com

difficult due to large distances of ULXs which are located in external galaxies, exhibiting a disk irradiation in a binary system. The observed optical candidates of ULXs are too faint ($m_V > 21$ mag.) to study in detail and confirm spectroscopically from the ground-based observations (Fabrika et al. 2015; Kaaret et al. 2017). However, there are several exceptions in which the type and mass of the donor star are determined by optical spectroscopy, for instance: in ULX-1 of M101, which has a Wolf-Rayet donor (Liu et al. 2013), M-type supergiant donors in ULX-1 of NGC 253, ULX-2 of NGC 925 and ULX-1 of NGC 4136 (Heida et al. 2015, 2016) and also P13 of NGC 7793 which is a PULX, with a blue supergiant donor of type B9Ia (Motch et al. 2011, 2014). In general, absolute magnitudes of ULXs, M_V , are in the range of -8 and -3 mag. (Vinokurov et al. 2018). Although there are hundreds of ULXs known, only about 20 have singled out optical counterparts (Tao et al. 2011; Gladstone et al. 2013; Avdan et al. 2019). For many other ULXs, multiple undecidable optical counterparts have been detected (Soria et al. 2005; Mucciarelli et al. 2007; Avdan et al. 2016b, 2019; Aksaker et al. 2019). Mostly, they have very faint optical candidates showing star-like spectral energy distributions (SEDs). Their SEDs are constructed by assuming that the optical emissions come from donor stars (Avdan et al. 2016a; Vinokurov et al. 2018).

NGC 1316 (also known as Fornax A) is a giant elliptical galaxy located in the outskirts of the Fornax galaxy cluster. In many studies, the distance of NGC 1316 was estimated with slightly different values from each other (e.g. Jensen et al. 2003; Feldmeier et al. 2007; Stritzinger et al. 2010; Cantiello et al. 2013; Hatt et al. 2018; Lakhchaura et al. 2018; Babyk et al. 2019). Throughout this work, we adopted the distance to the NGC 1316 as 19 Mpc (Jensen et al. 2003). In the radio band, NGC 1316 is one of the brightest galaxy in the sky, with giant double radio lobes and well defined core jet structure (Geldzahler & Fomalont 1984). The galaxy has an peculiar morphology with numerous tidal tails, shells and loops of interstellar medium (Schweizer 1980, 1981). NGC 1316 also displays dust patches in the central region together with the prominent dust lanes oriented along its optical minor axis (see Fig. 1).

In the previous studies, it is reported that the galaxy hosts many X-ray sources including several ULXs by using the archival *Chandra* and *XMM-Newton* data (Kim & Fabbiano 2003; Swartz et al. 2004; Liu 2011; Earnshaw et al. 2019). Based on *Chandra* observation of 2002, Kim & Fabbiano (2003) detected 81 point sources within the 25th magnitude isophotal ellipse of NGC 1316. According to their source list, they reported only one potential ULX source (#29) even though three more sources (#12, #13 and #44) have luminosities $\geq 10^{39}$ erg s $^{-1}$. They also reported that the luminosity of the #13 is highly uncertain due to the contamination of the X-ray diffuse emission and remaining two sources are located at the center of galaxy with elongated shapes and uneasy source definitions. On the other hand, Liu (2011) analyzed the same data and determined 4 ULXs in NGC 1316. These ULXs were X-3 (#16), X-6 (#64), X-5 (#13) and X-4 (#29) with numbering by their maximum detection significance. Recently, Earnshaw et al. (2019) have reported the aforementioned ULX candidates by using *XMM-Newton* data.

In the present study, we report the identification of the X-ray source CXOUJ032240.8-371224 as a new ULX to be denoted as ULX X-7 (hereafter X-7) as a result of the analysis of 2019 *Chandra* data. We obtained the peak luminosity of X-7 as 2×10^{39} erg s $^{-1}$ in the energy of 0.3–8 keV with adopted distance 19 Mpc. However, this source has earlier been cataloged as #14 by Kim & Fabbiano (2003) with a luminosity of $\sim 5.75 \times 10^{38}$ erg s $^{-1}$ in the same energy range. We further investigated the X-ray spectral and temporal properties of X-7. We also identified a single

optical counterpart of this source using the *HST* multi-band optical observations.

The present paper is organized as follows: *Chandra* and *HST* data reductions and analysis are presented in Section 2. The results of the analysis and discussions are given in Section 3.

2 OBSERVATIONS, DATA REDUCTION AND ANALYSIS

2.1 X-rays

NGC 1316 was observed by *Chandra* ACIS-S once in 2001, and five times in April 2019. In addition, this galaxy was observed four times by *XMM-Newton* in 2005 but only two of the *XMM-Newton* observations included the position of X-7. There were numerous observations of NGC 1316 obtained by *Swift-XRT* between 2006 and 2020. However, the source X-7 could not be resolved clearly in both observations. Therefore, only the data taken with *Chandra* ACIS-S observations were used in the present study. The log of observations is given in Table 1.

Chandra data were analyzed by using CIAO¹ v4.12 software with its calibration package CALDB² v4.9. Several X-ray sources were detected from level 2 event list using WAVDETECT tool in CIAO. We determined a new coordinates for X-7 as R.A. = $03^h22^m40^s.813$ and Dec. = $-37^\circ12'23''.47$ by using C6 data. The differences between the early coordinates given by Kim & Fabbiano (2003) were $\sim 0''.20$ for R.A and $0''.53$ for Dec. The new ULX source X-7 is located $12''$ away from center of the galaxy. The position of this source is shown on the *Chandra* and *HST* images in Fig. 1.

The source and background photons were extracted with SPEXTRACT task using a circle with a radius of $2''.5$. The spectral analyses of the X-ray data have been performed by using the package, XSPEC v12.11. We only used observations labeled as C5 (ObsID 20341) and C6 (ObsID 22187) for the spectral analyses due to the low statistics (≤ 50 counts) of other *Chandra* 2019 observations.

Several single component models such as absorbed power-law (PL), multi-color disk blackbody (DISKBB) and blackbody (BODY) were fitted to the spectra of X-7. We also fitted the source spectra with the frequently used two-component models such as DISKBB + PL and DISKBB + COMPTT; however, no statistically significant improvement was achieved for C5 and C6 data. Hence, we will not discuss the two component models any further in this work.

In our initial fits, each model included two absorption components: The first one was a fixed Galactic column density of $N_H = 2 \times 10^{20}$ cm $^{-2}$ (Dickey & Lockman 1990) representing the absorbing line-of-sight column density along to the NGC 1316 (using the TBABS model) and the other one was left free to account for intrinsic absorption. The later component was found to be negligible in the resulting fitting parameters. The unabsorbed flux was calculated in the 0.3–10 keV energy band using the convolution model CFLUX available in XSPEC and the corresponding luminosity value was calculated using the distance of 19 Mpc. Due to the relatively low source counts for C5 (88 net counts) and C6 (102 net counts) observations we used the Cash statistic (or C-stat; Cash 1979) for spectral fitting. The spectra were grouped at least of 5 counts per bin. The resulting spectral parameters of single-component models for C5 and C6 data are given in Table 2.

In order to search for any periodicity, C6 data were used to perform a timing analyses since it provides better statistics than

¹ <https://cxc.cfa.harvard.edu/ciao/>

² <https://cxc.cfa.harvard.edu/caldb/>

others. The X-ray light curve of X-7 was sampled at 3.2 s using DMEXTRACT tool in CIAO and power density spectra (PDS) were calculated using XRONOS v6.0 in HEASOFT v6.27. The PDS were calculated from a single interval or up to six spectra were averaged to produce a PDS in the 0.3–10 keV band. We cannot confirm any significant ($\geq 3\sigma$) periodicity with time-bin size of 3.2 s which sets a lower limit for searching periods.

2.2 HST

The archival data log of Hubble Space Telescope³ (*HST*) observations used for analysis are given in Table 1. We performed a relative astrometry between *Chandra* (ObsID 22187) and the *HST*/ACS (Advanced Camera for Surveys) (ObsID j6n202010) images to find the optical candidate of X-7. We used CIAO/wavedetect and IRAFdaofind tools for source detection in *Chandra* and *HST*/ACS images, respectively.

Nine reference sources were determined from the comparison of the *Chandra* and *HST* images. All of these matched sources are located on ACIS-S with a moderate offset from the optical axis in the ObsID 22187. Properties of reference sources are summarized in Table 3. The position uncertainties between each of reference sources were calculated with 90% confidence level. The final astrometric errors between the *Chandra* and *HST* images are in R.A. 0''09 and in Dec. 0''07. As a result of astrometric correction, the *HST* coordinates of X-7 are given as R.A. = 03^h22^m40^s.806 and Dec. = 37°12'23''.52 within 95 % confidence level of error circle with 0''22 radius.

The Point-Spread Function (PSF) photometry was performed with DOLPHOT v2.0 (Dolphin 2000) using the *HST* data (*.flt.fits and *.drz.fits) listed in Table 1. The ACSMASK task was used to remove pixels flagged as bad in *.flt images. SPLITGROUPS and CALSKY tasks were performed to split into single-chip images and were created the sky background for each image, respectively. Here, we present the magnitudes derived by using the set of parameters for the ACS, WFC3/UVIS and WFC3/IR recommended by DOLPHOT user's guide. The DOLPHOT task was used for photometry by taking drizzled images ObsID j6n202010 and ObsID ib3n03030 as the positional reference for both ACS and WFC3, respectively.

We found a unique optical candidate within 0''22 error circle at 95% confidence level for X-7 using the archival *HST*/ACS and *HST*/WFC3 data (see 1). The ACS and WFC3 magnitudes in the VegaMag. and Johnson system for the optical candidate are given in Table 4. Magnitude values were corrected with $E(B - V) = 0.018$ mag. derived from the Galactic extinction ($A_V/3.1$). The $A_V = 0.058$ mag. was obtained from extinction calculator tools of NED⁴. The F475W, F555W and F814W filters in *HST*/ACS correspond to the Johnson filter *B*, *V* and *I*, respectively (Sirianni et al. 2005; Saha et al. 2011). We obtained $B - V = 0.77$ mag., $V - I = 1.10$ mag. and $M_V = -7.80$ mag. The distance modulus of NGC 1316 is calculated as 31.4 mag. by using the adopted distance of 19 Mpc.

Spectral Energy Distribution (SED) of the optical candidate has been constructed to obtain the spectral characteristics of X-7 using the derived flux values given in Table 1. The wavelength of the filters are selected as the pivot wavelength, obtained from PYSYNPHOT⁵, in SED plots. The SED for the optical candidate is adequately fitted (1) a blackbody spectrum with a temperature of

3100 ± 400 K or (2) a power-law spectrum ($F \propto \lambda^\alpha$) with $\alpha = 1.75 \pm 0.35$, see Fig. 2. To obtain a blackbody spectrum, a code has been used with OPTIMSET and FMINSEARCH functions in MATLAB⁶. The reduced χ^2 for blackbody and power-law are 1.34 and 1.27, respectively. The number of degrees of freedom is four for both models.

3 RESULTS AND DISCUSSIONS

3.1 X-Rays

We identified a new ULX in NGC 1316 by *Chandra* in April 2019 with a luminosity of 2.10×10^{39} erg s⁻¹. This luminosity is almost a factor of ~ 4 times higher than previous *Chandra* observation in April 2001. We obtained the best-fitting spectral parameters of one-component models for X-7 to elaborate its spectral characteristics. These parameters were obtained with only one intrinsic absorption, $N_H = 2 \times 10^{20}$ cm⁻² since the second absorption parameter did not contribute significantly. The spectra of X-7 are the best fitted by PL models with photon indices of $\Gamma = 2.24$ for C5 and 1.56 for C6 data. The source has maximum unabsorbed luminosity values of ~ 1.8 and 2.1×10^{39} in 0.3–10 keV, respectively. These values are also listed in Table 2. Energy spectrum of X-7 with a PL model and its residual are shown in Fig. 3. The source spectra were also fitted by the DISKBB model with $T_{in} = 0.78$ keV (C5) and 1.32 keV (C6). The other well fitted model is BBODY whose temperature values are 0.50 keV and 0.74 keV with unabsorbed luminosities 0.92 and 1.21×10^{39} erg s⁻¹ for C5 and C6, respectively. As noted, it is difficult to differentiate between these three models due to their very similar C-stat.

We also searched for short-term and long-term count rate variability. For the short-term variability, the light curve of X-7 was binned over intervals of 100s, 500s and 1000s in the 0.3–10 keV energy band using C6 data. The resulting light curves were tested for short-term variations in the source count rates using a Kolmogorov-Smirnov (K-S) test. The K-S test probabilities are found as > 0.3 . These results indicate that X-7 do not show any significant amplitude variations.

Bi-modal distribution obtained from the long-term light curves is considered to be a good indication of the presence of a neutron star in ULXs (Earnshaw et al. 2018; Song et al. 2020; Pintore et al. 2020; Brightman et al. 2020). Therefore, we also checked the long-term variability of X-7, for this we used equation of Brightman et al. (2020). According to their definition the count rate variability is determined the equality by $\chi_r^2 \equiv \chi^2 / N_{obs}$, where χ_r^2 is an arbitrary definition of count rate variability and N_{obs} is the number of observations. In their work, when $\chi_r^2 > 2$ the source is considered to be variable. They applied this formula to their sources in M51 (Brightman et al. 2020) and obtained χ_r^2 is about 10 for (ULX X-7 and ULX X-8). Then, they considered these two sources strongly variable. We found that $\chi_r^2 \approx 5$ for all *Chandra* observations and comparing our value with theirs, X-7 of NGC 1316 is also probably mildly variable. Due to the fact that, more observations are required to interpret the long-term variability of X-7 might point out a neutron star in ULX system.

In the spectral analyses of the *Chandra* data, we found that the spectra of X-7 in C5 and C6 are better represented by PL models with photon indices $\Gamma \sim (2.24 \text{ and } 1.56)$. Both of these Γ values

³ <https://archive.stsci.edu/hst/search.php>

⁴ https://ned.ipac.caltech.edu/extinction_calculator

⁵ <https://pysynphot.readthedocs.io/en/latest/>

⁶ <https://www.mathworks.com/matlabcentral/fileexchange/20129-fit-blackbody-equation-to-spectrum>

correspond to hard states defined for GBHBs. Hard states with low luminosity are seen at sub-Eddington mass accretion rates. On the other hand, `DISKBB` model also yields acceptable fits for the same datasets with the temperature of $kT_{in} \sim (0.78 \text{ and } 1.32) \text{ keV}$. These kT_{in} values are compatible with those of GBHBs at a high mass accretion rate during thermal state (Remillard & McClintock 2006). Generally in GBHBs, luminosities are usually hard when they are bright and soft when they are dim. However, X-7 exhibits the opposite behavior since the source has a high L_X when it is in a hard state and a low L_X when it is in a soft state. There are some ULXs that do show similar correlations like X-2 of NGC 1313, Feng & Kaaret (2006); X-1 of IC 342, Marlowe et al. (2014); X-2 of NGC 4736, Avdan et al. (2014). X-3 of NGC 925, Earnshaw et al. (2020). We used the normalization parameter of the `diskbb` model in C6 data to constrain the mass of the compact object. Here, we found an apparent inner disk radius of $r_{in} \sqrt{\cos 60} \approx 59 \text{ km}$. The apparent radius was corrected to the true value using the equation of $R_{in} = r_{in} \kappa^{-2} \xi$, where $\xi = 0.412$ is the correction factor and $\kappa = 1.7$ is spectral hardening factor (Shimura & Takahara 1995; Kubota et al. 1998) and the resultant $R_{in} \sim 70 \text{ km}$. Using the relation between inner disk radius and mass (Makishima et al. 2000), we found $M \sim 8 M_\odot$ for the mass of compact object in X-7.

As discussed in several studies, when the data quality is low and exposure is short, one-component models should be taken into account with care due to low statistics. However, these models do not provide physically sufficient detail to interpret the data (Gladstone et al. 2009; Sutton et al. 2013; Kaaret et al. 2017).

We also examined if luminosities of the ULXs (X-3, X-5 and X-4) in NGC 1316 given by (Liu 2011), vary or not. We performed spectral analyses of these ULXs by using C6 data. The unabsorbed X-ray luminosity L_X was calculated with an `PL` model in 0.3–8.0 keV adopted distance 19 Mpc for each of three sources. Resulting L_X values are 4.11, 2.52, and $4.01 \times 10^{39} \text{ erg s}^{-1}$ for X-3, X-5 and X-4, respectively. Variation of the L_X values for these ULXs were found less than a factor two on a timescale of 18 years.

In addition, we determined a source located at $\sim 6''$ southwest of the X-7 at R.A. = $3^h 22^m 40^s.550$ and Dec. = $-37^\circ 12' 26''.45$ (see Fig. 1). This source is also in the list of Kim & Fabbiano (2003) as CXOU J032240.571227 (#16) with a luminosity of $3.34 \times 10^{38} \text{ erg s}^{-1}$. The source count rates for all data (C1–C6) were obtained fitting an absorbed `PL` model with same $N_H = 2 \times 10^{20} \text{ cm}^{-2}$ the $\Gamma = 1.7$ and resulting unabsorbed fluxes were obtained by using `SRCFLUX` tool in `CIAO` at 90% confidence level in the range of 0.3–10 keV. The flux values of C2 and C4 data were found as $0.16 \times 10^{-14} \text{ erg cm}^{-2} \text{ s}^{-1}$ (minimum) and $2.31 \times 10^{-14} \text{ erg cm}^{-2} \text{ s}^{-1}$ (maximum). This maximum flux corresponds to luminosity of $\sim 1.0 \times 10^{39} \text{ erg s}^{-1}$. We note that, the flux variation of the source is a quite significant with an order of magnitude difference. Due to the variation, this source could be a candidate of transient ULX which we named as XT-1, as seen clearly in Fig. 4.

3.2 HST

We examined the optical properties of X-7 in the galaxy NGC 1316 using the archival data from *HST*/ACS and *HST*/WFC3. A unique optical candidate was identified within $0.''22$ error radius after the astrometric correction. It is noted that dereddened magnitudes of optical candidate are faint ($m_V > 22.5 \text{ mag}$) as seen in Table 4. On the other hand, the absolute magnitude is very bright $M_V = -7.80 \text{ mag}$ which is the compatible with the given range ($-4 < M_V < -9$) for ULXs (Gladstone et al. 2013).

We fitted a blackbody and power-law model to SED of X-7 as

seen in Fig 2. The best-fitting parameter for power-law model is $\alpha = 1.75 \pm 0.35$ and the temperature is $3100 \pm 400 \text{ K}$ for blackbody model. Although, both model yields similar reduced $\chi^2 \approx 1.3$, the α parameter for power-law is not in the range of -3 and -4 . This range is given for optical counterparts of many ULXs having power-law SEDs (Tao et al. 2011; Vinokurov et al. 2018). It follows that the blackbody model is more favorable. If so, the blackbody emission is thought to originate from the companion star via irradiation the accretion disk with an emission radius of $\approx 2 \times 10^{13} \text{ cm}$. This radius is an order of magnitude greater than the acceptable radius for ULXs. However, the very similar radius was also reported for X-1 of IC 342 (Tao et al. 2011). Moreover, the SED of X-7 is also similar to X-1 of IC 342 (Tao et al. 2011). In their work, they also fitted these two models and showed that their data is better fitted to the blackbody model. According to Straizys & Kuriliene (1981) the measured temperature and luminosity of the companion star indicate that spectral classification would be an M type supergiant. Similar spectral type of companions are proposed for ULX-5 of NGC 3034, ULX-1 and ULX-2 of NGC 253 by Gladstone et al. (2013).

We have also examined whether the size of the emitting region can reprocess this optical emission. Assuming a fraction η of the X-ray luminosity, L_X , is reprocessed with $\eta = \sigma T^4 A / L_X$ where σ , T and A are Stefan-Boltzmann constant, temperature and area of the region, respectively. Inserting $T = 3100 \text{ K}$, $A \sim 10^{27} \text{ cm}^2$, and $L_X = 2 \times 10^{39} \text{ erg cm}^{-2} \text{ s}^{-1}$, we found that η is ≈ 0.002 which is similar value for the GBHBs such as XTE J1817–330 and X-1 of Holmberg IX (Gierliński et al. 2009; Tao et al. 2011).

In addition, we investigated the optical candidates of previously known ULXs (X-3, X-4 and X-5) from study of Liu (2011) and also the XT-1 in the NGC 1316. As noted, we identified a single optical candidate for X-5 located at the edge of the $0.''22$ error circle. Its V-band magnitude is $23.1 \pm 0.03 \text{ mag}$. This candidate is not associated with any source in the CDS (Centre de Données astronomiques de Strasbourg) database. On the other hand, the source XT-1 has no optical counterpart(s) in *HST* images.

As a conclusion, further broadband X-ray observations of X-7 are needed to constrain the spectral parameters better and scale of variability of the source with more confidence. It will allow us to interpret mechanisms of X-ray emission from accretion processes in ULXs. Rising from obscurity to super-Eddington luminosities with several examples: (1) from this work, (2) from Pintore et al. (2018) and probably others may give us new clues to better understand the nature of ULXs.

ACKNOWLEDGEMENTS

This research was supported by the Scientific and Technological Research Council of Turkey (TAİJBRTAK) through project number 117F115. This research was also supported by the Gukurova University Research Fund through project number FBA-2019-11803. This research is a part of the PhD thesis of S.A. We special thanks to M. E. Ozel for his valuable contribution of the manuscript.

REFERENCES

- Aksaker N., Akyuz A., Avdan S., Avdan H., 2019, *MNRAS*, **488**, 5935
- Avdan H., Kayaci Avdan S., Akyuz A., Balman S., 2014, *Ap&SS*, **352**, 123
- Avdan S., et al., 2016a, *MNRAS*, **455**, L91
- Avdan H., Avdan S., Akyuz A., Balman S., Aksaker N., Akkaya Oralhan I., 2016b, *ApJ*, **828**, 105

- Avdan S., et al., 2019, *ApJ*, **875**, 68
- Babik I. V., McNamara B. R., Tamhane P. D., Nulsen P. E. J., Russell H. R., Edge A. C., 2019, *ApJ*, **887**, 149
- Bachetti M., et al., 2013, *ApJ*, **778**, 163
- Bachetti M., et al., 2014, *Nature*, **514**, 202
- Brightman M., et al., 2018, *ApJ*, **867**, 110
- Brightman M., et al., 2020, *ApJ*, **895**, 127
- Cantiello M., et al., 2013, *A&A*, **552**, A106
- Carpano S., Haberl F., Maitra C., Vasilopoulos G., 2018, *MNRAS*, **476**, L45
- Cash W., 1979, *ApJ*, **228**, 939
- Colbert E. J. M., Mushotzky R. F., 1999, *ApJ*, **519**, 89
- Dickey J. M., Lockman F. J., 1990, *ARA&A*, **28**, 215
- Dolphin A. E., 2000, *PASP*, **112**, 1383
- Earnshaw H. P., Roberts T. P., Sathyaprakash R., 2018, *MNRAS*, **476**, 4272
- Earnshaw H. P., Roberts T. P., Middleton M. J., Walton D. J., Mateos S., 2019, *MNRAS*, **483**, 5554
- Earnshaw H. P., et al., 2020, *ApJ*, **891**, 153
- Fabrika S., Ueda Y., Vinokurov A., Sholukhova O., Shidatsu M., 2015, *Nature Physics*, **11**, 551
- Feldmeier J. J., Jacoby G. H., Phillips M. M., 2007, *ApJ*, **657**, 76
- Feng H., Kaaret P., 2006, *ApJ*, **650**, L75
- Fürst F., et al., 2016, *ApJ*, **831**, L14
- Fürst F., Walton D. J., Stern D., Bachetti M., Barret D., Brightman M., Harrison F. A., Rana V., 2017, *ApJ*, **834**, 77
- Geldzahler B. J., Fomalont E. B., 1984, *AJ*, **89**, 1650
- Gierliński M., Done C., Page K., 2009, *MNRAS*, **392**, 1106
- Gladstone J. C., Roberts T. P., Done C., 2009, *MNRAS*, **397**, 1836
- Gladstone J. C., Copperwheat C., Heinke C. O., Roberts T. P., Cartwright T. F., Levan A. J., Goad M. R., 2013, *ApJS*, **206**, 14
- Hatt D., et al., 2018, *ApJ*, **866**, 145
- Heida M., et al., 2015, *MNRAS*, **453**, 3510
- Heida M., Jonker P. G., Torres M. A. P., Roberts T. P., Walton D. J., Moon D. S., Stern D., Harrison F. A., 2016, *MNRAS*, **459**, 771
- Israel G. L., et al., 2017a, *Science*, **355**, 817
- Israel G. L., et al., 2017b, *MNRAS*, **466**, L48
- Jensen J. B., Tonry J. L., Barris B. J., Thompson R. I., Liu M. C., Rieke M. J., Ajhar E. A., Blakeslee J. P., 2003, *ApJ*, **583**, 712
- Kaaret P., Feng H., Roberts T. P., 2017, *ARA&A*, **55**, 303
- Kim D.-W., Fabbiano G., 2003, *ApJ*, **586**, 826
- Kubota A., Tanaka Y., Makishima K., Ueda Y., Dotani T., Inoue H., Yamaoka K., 1998, *PASJ*, **50**, 667
- Lakhchaura K., et al., 2018, *MNRAS*, **481**, 4472
- Liu J., 2011, *ApJS*, **192**, 10
- Liu J.-F., Bregman J. N., Bai Y., Justham S., Crowther P., 2013, *Nature*, **503**, 500
- Luangtip W., Roberts T. P., Done C., 2016, *MNRAS*, **460**, 4417
- Madau P., Rees M. J., 2001, *ApJ*, **551**, L27
- Makishima K., et al., 2000, *ApJ*, **535**, 632
- Marlowe H., et al., 2014, *MNRAS*, **444**, 642
- Mezcua M., Roberts T. P., Lobanov A. P., Sutton A. D., 2015, *MNRAS*, **448**, 1893
- Motch C., Pakull M. W., Grisé F., Soria R., 2011, *Astronomische Nachrichten*, **332**, 367
- Motch C., Pakull M. W., Soria R., Grisé F., Pietrzyński G., 2014, *Nature*, **514**, 198
- Mucciarelli P., Zampieri L., Treves A., Turolla R., Falomo R., 2007, *ApJ*, **658**, 999
- Pintore F., Zampieri L., Stella L., Wolter A., Mereghetti S., Israel G., 2017, in Ness J.-U., Migliari S., eds, *The X-ray Universe 2017*. p. 314
- Pintore F., et al., 2018, *MNRAS*, **477**, L90
- Pintore F., et al., 2020, *ApJ*, **890**, 166
- Poutanen J., Fabrika S., Valeev A. F., Sholukhova O., Greiner J., 2013, *MNRAS*, **432**, 506
- Remillard R. A., McClintock J. E., 2006, *ARA&A*, **44**, 49
- Roberts T. P., 2007, *Ap&SS*, **311**, 203
- Rodríguez Castillo G. A., et al., 2019, arXiv e-prints, p. [arXiv:1906.04791](https://arxiv.org/abs/1906.04791)
- Saha A., Shaw R. A., Claver J. A., Dolphin A. E., 2011, *PASP*, **123**, 481
- Sathyaprakash R., et al., 2019, *MNRAS*, **488**, L35
- Schweizer F., 1980, *ApJ*, **237**, 303
- Schweizer F., 1981, *ApJ*, **246**, 722
- Shimura T., Takahara F., 1995, *ApJ*, **445**, 780
- Sirianni M., et al., 2005, *PASP*, **117**, 1049
- Song X., Walton D. J., Lansbury G. B., Evans P. A., Fabian A. C., Earnshaw H., Roberts T. P., 2020, *MNRAS*, **491**, 1260
- Soria R., Cropper M., Pakull M., Mushotzky R., Wu K., 2005, *MNRAS*, **356**, 12
- Stobart A. M., Roberts T. P., Wilms J., 2006, *MNRAS*, **368**, 397
- Straizys V., Kuriliene G., 1981, *Ap&SS*, **80**, 353
- Stritzinger M., et al., 2010, *AJ*, **140**, 2036
- Sutton A. D., Roberts T. P., Middleton M. J., 2013, *MNRAS*, **435**, 1758
- Swartz D. A., Ghosh K. K., Tennant A. F., Wu K., 2004, *ApJS*, **154**, 519
- Tao L., Feng H., Grisé F., Kaaret P., 2011, *ApJ*, **737**, 81
- Vinokurov A., Fabrika S., Atapin K., 2018, *ApJ*, **854**, 176

This paper has been typeset from a \LaTeX file prepared by the author.

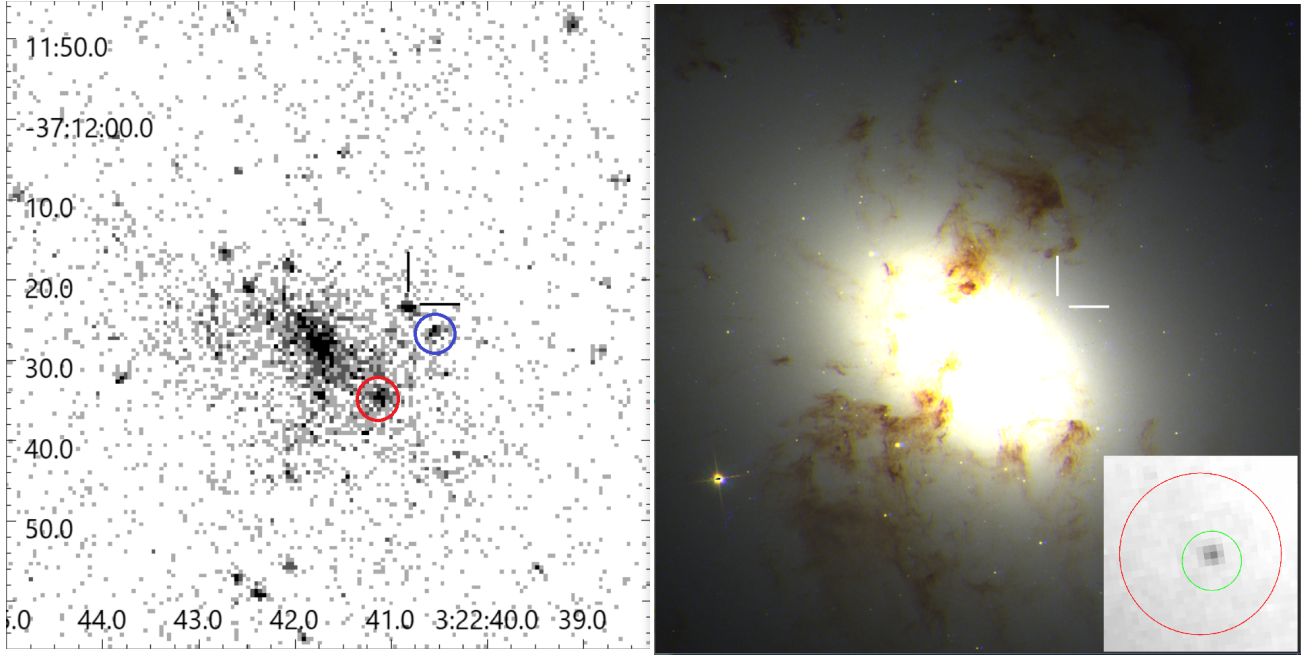


Figure 1. Left panel: *Chandra*/ACIS-S image of the galaxy NGC 1316. The black bars (5'') show the location of ULX X-7. Red and blue circles represent the ULX X-5 and transient source XT-1, respectively. Right panel: *HST* image of the X-7 with RGB (Red: ACS/F814W, Green: ACS/F555W and Blue: WFC3/F336W). The position of X-7 is marked with white bars. An inset representing inverted color *HST*/ACS/F555W image of the X-7. The red and green circles represent the *Chandra* position of X-7 with a radius of 0.''6 and the corrected position of X-7 with an error radius of 0.''22, respectively. Both panels show exactly the same region. X and Y axis represent R.A. and Dec. respectively. The north is up and the east is left.

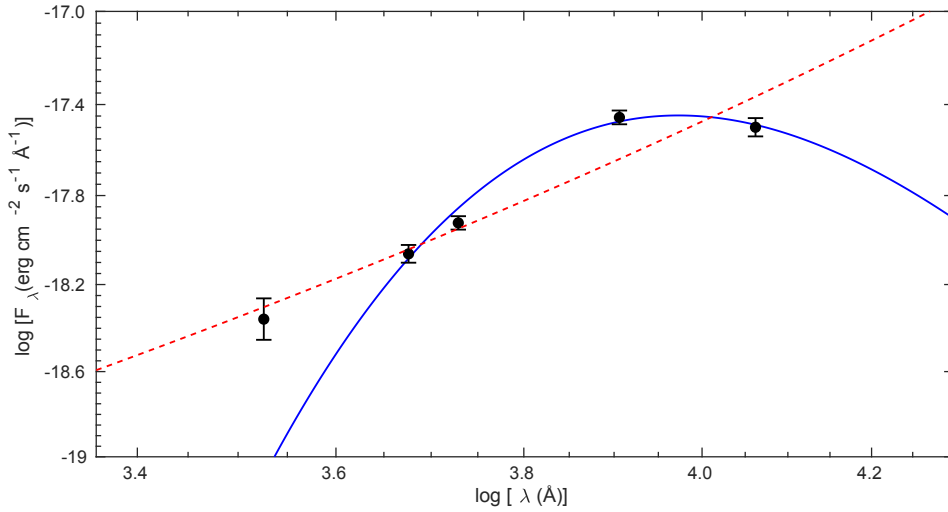


Figure 2. The SED of optical candidate of X-7. All data are shown with black circles and their respective error with bars. The SED models are shown by blue solid line for blackbody and red dashed line for power-law. The blackbody has a temperature of 3100 ± 400 K and the power-law model is $\alpha = 1.75 \pm 0.35$ for the X-7.

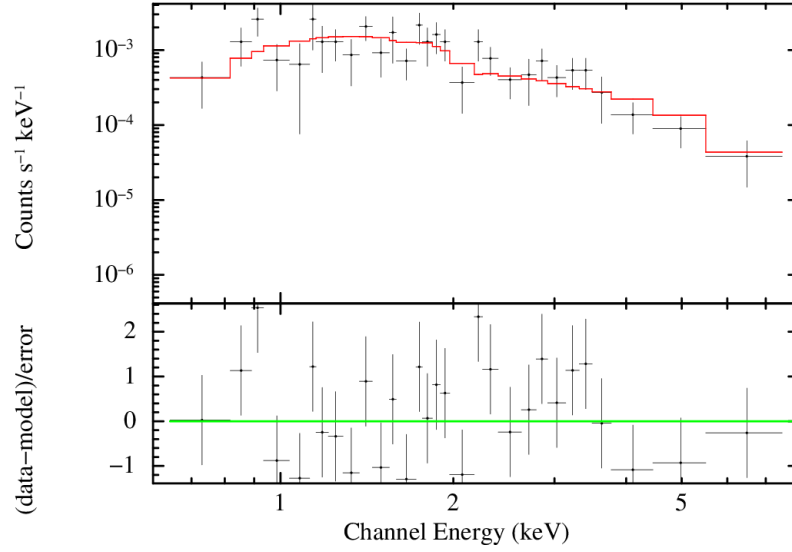


Figure 3. Energy spectrum of X-7 obtained using C6 data, the spectrum was fitted with PL model. The *Chandra* spectrum and fitting model are shown in black and red colors, respectively. The upper panel shows the data and best fitting model. The lower panel shows the residual.

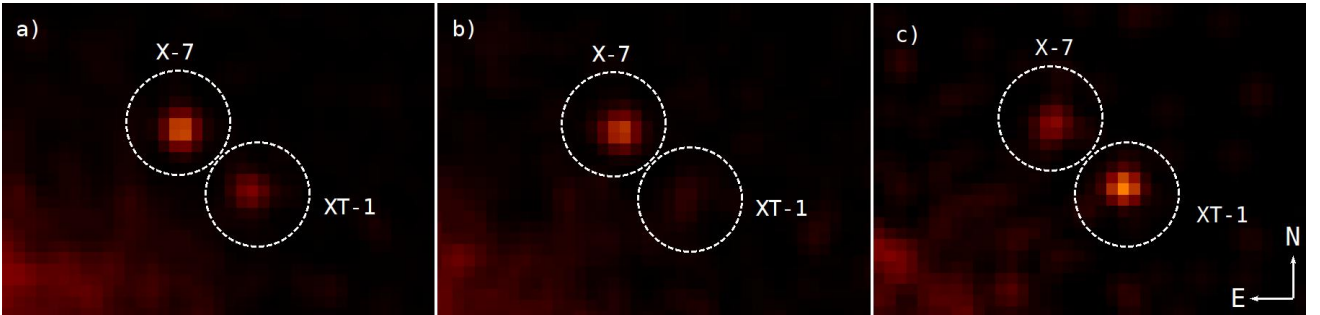


Figure 4. Comparison of X-7 and XT-1 in the *Chandra* observations (C1:a, C2:b and C4:c). The X-7 and XT-1 positions are represented with dashed white circles. The XT-1 lies at $\sim 6''$ to X-7. It is clearly seen that XT-1 is not detected in the C2 observation. The same region of $19'' \times 16''$ are given in all panels.

Table 1. The log of X-ray and optical observations of X-7

Instruments	Label/Filter	ObsID	Date	Exp.(ks)
<i>Chandra</i> /ACIS-S	C1	2022	2001-04-17	29.85
<i>Chandra</i> /ACIS-S	C2	20340	2019-04-16	44.97
<i>Chandra</i> /ACIS-S	C3	22179	2019-04-17	38.95
<i>Chandra</i> /ACIS-S	C4	22180	2019-04-20	13.57
<i>Chandra</i> /ACIS-S	C5	20341	2019-04-22	51.39
<i>Chandra</i> /ACIS-S	C6	22187	2019-04-25	53.18
<i>HST</i> /ACS/WFC	F555W	j6n202010	2003-03-04	6.98
<i>HST</i> /ACS/WFC	F814W	j6n201030	2003-03-07	2.20
<i>HST</i> /ACS/WFC	F475W	j90x01020	2005-02-16	0.76
<i>HST</i> /WFC3/UVIS	F336W	ib3n03040	2010-07-30	3.23
<i>HST</i> /WFC3/IR	F110W	ib3n03030	2010-07-30	0.40

Table 2. X-ray spectral fitting parameters of X-7.

Data	Model Name	Γ (keV)	$T_{in(DISKBB)}/kT(BBODY)$ (keV)	$N_{(PL)}^1$ (10^{-6})	$N_{(DISKBB)}^2$ (10^{-4})	$N_{(BBODY)}^3$ (10^{-7})	C/dof^4 ($10^{39} \text{ erg s}^{-1}$)	L_X^5
C5	PL	$2.24^{+0.37}_{-0.36}$	–	$8.07^{+2.13}_{-1.82}$	–	–	23.79/21(1.13)	$1.77^{+0.27}_{-0.23}$
	DISKBB	–	$0.78^{+0.07}_{-0.06}$	–	$0.31^{+0.05}_{-0.05}$	–	21.11/21(1.01)	$1.10^{+0.17}_{-0.13}$
	BBODY	–	$0.50^{+0.07}_{-0.06}$	–	–	$2.57^{+0.45}_{-0.40}$	25.80/21(1.23)	$0.92^{+0.11}_{-0.07}$
C6	PL	$1.56^{+0.29}_{-0.27}$	–	$5.20^{+1.42}_{-1.30}$	–	–	27.58/27(1.02)	$2.10^{+0.29}_{-0.26}$
	DISKBB	–	$1.32^{+0.51}_{-0.27}$	–	$4.80^{+0.76}_{-0.76}$	–	24.71/27(0.92)	$1.47^{+0.23}_{-0.20}$
	BBODY	–	$0.74^{+0.11}_{-0.10}$	–	–	$3.35^{+0.68}_{-0.58}$	26.14/27(0.96)	$1.21^{+0.23}_{-0.19}$

Notes: A fixed $N_H = 2 \times 10^{20}$ was used in all models.

¹ PL model normalization parameter. ² DISKBB model normalization parameter; $N = (r_{in} / D_{10})^2 \times \cos\theta$, where r_{in} is the apparent inner disk radius, D is the distance to the source in units of 10 kpc, and θ is the inclination of the disk. ³ BBODY model normalization parameter. ⁴ C-statistic of the fit and the number of degrees of freedom. ⁵ The unabsorbed luminosity were calculated in energy range of 0.3-10 keV with adopted distance 19 Mpc.

Table 3. Coordinates of the X-ray/optical reference sources. *Chandra* ACIS-S sources (ObsID 22187) identified in *HST* data (j6n202010).

<i>Chandra</i> R.A. (hh:mm:ss.sss)	<i>Chandra</i> Dec. (° : ' : ")	Net Counts ^a –	<i>HST</i> R.A. (hh:mm:ss.sss)	<i>HST</i> Dec. (° : ' : ")	Position Uncertainty ^b (")
3:22:42.719	-37:12:16.63	39.20 ± 7.00	3:22:42.728	-37:12:16.60	0.16
3:22:42.066	-37:12:18.23	36.11 ± 7.14	3:22:42.055	-37:12:18.26	0.13
3:22:42.484	-37:12:21.06	56.50 ± 9.11	3:22:42.457	-37:12:20.99	0.37
3:22:42.596	-37:12:06.32	8.92 ± 3.16	3:22:42.600	-37:12:06.24	0.11
3:22:41.153	-37:11:43.92	15.70 ± 4.58	3:22:41.172	-37:11:44.26	0.48
3:22:41.318	-37:11:17.09	22.02 ± 5.00	3:22:41.297	-37:11:17.13	0.29
3:22:39.123	-37:11:47.97	66.18 ± 8.49	3:22:39.120	-37:11:48.00	0.05
3:22:37.710	-37:12:51.05	18.11 ± 4.47	3:22:37.690	-37:12:51.13	0.28
3:22:44.729	-37:13:10.03	09.76 ± 3.32	3:22:44.713	-37:13:10.09	0.22

^a The counts were calculated in the 0.3-10 keV using XSPEC.

^b Uncertainties are given at 90% confidence level of the *Chandra/HST* reference sources.

Table 4. The dereddened *HST* magnitudes and color values of optical candidate of X-7.

Instruments	Date (yyyy-mm-dd)	Filter	Pivot Wavelength [*] (Å)	VegaMag	JohnsonMag	Flux $10^{-18} \text{ (erg cm}^{-2} \text{ s}^{-1} \text{ Å}^{-1})$
ACS	2005-02-16	F475W	4746.7	24.05 ± 0.06	(B) 24.40 ± 0.06	0.86 ± 0.02
	2003-03-04	F555W	5360.8	23.70 ± 0.03	(V) 23.63 ± 0.03	1.19 ± 0.01
	2003-03-07	F814W	8044.8	22.54 ± 0.02	(I) 22.53 ± 0.02	3.49 ± 0.01
WFC3					$(B - V)_0 = 0.77$	
					$(V - I)_0 = 1.10$	
					$M_V = -7.80$	
WFC3	2010-07-30	F336W	3354.8	24.79 ± 0.21	–	0.43 ± 0.08
	2010-07-30	F110W	11534.5	22.64 ± 0.15	–	3.16 ± 0.02

^{*} The Pivot Wavelengths were calculated using *pysynphot*.